

Primljen / Received: 23.3.2016.

Ispravljen / Corrected: 5.8.2016.

Prihvaćen / Accepted: 1.9.2016.

Dostupno online / Available online: 10.10.2016.

Discrete dome model for St. Jacob cathedral in Šibenik

Authors:



Dalibor Gelo, MCE

Technical college in Zagreb
Department of Civil Engineering
dgelo@tvz.hr



Prof. **Mladen Meštrović**, PhD. CE
University of Zagreb
Faculty of Civil Engineering
mestar@grad.hr

Preliminary report

Dalibor Gelo, Mladen Meštrović

Discrete dome model for St. Jacob cathedral in Šibenik

Principal features of the non-smooth contact dynamics method, which served as basis for the LMGC90 software formulation, are presented in the paper. The objective of the paper is to present creation of a discrete model using the LMGC90 software. The discrete dome model of the St. Jacob cathedral in Šibenik was created, and dynamic behaviour of the dome was checked by time-history analysis. The results point to a highly nonlinear behaviour of the dome, which would be difficult to detect with the finite element method. The results also reveal critical points, i.e. the maximum displacement and contact force points along the dome.

Ključne riječi:

discrete element, non-smooth contact dynamics, LMGC90, contact law, Gauss-Seidel

Prethodno priopćenje

Dalibor Gelo, Mladen Meštrović

Diskretni model kupole katedrale svetoga Jakova u Šibeniku

U radu su prikazane osnove metode neglatke kontaktne dinamike na temelju koje je formuliran programski paket LMGC90. Cilj rada je prezentirati postupak izrade diskretnog modela u programu LMGC90. Izrađen je diskretni model kupole katedrale sv. Jakova u Šibeniku i na njemu je provedena time-history analiza. Dobiveni rezultati upućuju na značajna nelinearna ponašanja kupole koja je teško obuhvatiti metodom konačnih elemenata. Rezultati upućuju na kritična mjesta, to jest locirana su područja maksimalnih pomaka i kontaktnih sila.

Ključne riječi:

diskretni element, neglatka kontaktna dinamika, LMGC90, kontaktni zakon, Gauss-Seidel

Vorherige Mitteilung

Dalibor Gelo, Mladen Meštrović

Diskretes Modell der Kuppel der Kathedrale des Heiligen Jakob in Šibenik

In dieser Arbeit werden die Grundsätze der nicht-glatte Kontaktdynamik, auf die sich das Softwarepaket LMGC90 stützt, dargestellt. Das Ziel der Arbeit ist, den Aufbau eines diskreten Modells im Programm LMGC90 darzustellen. Ein diskretes Modell der Kuppel der Kathedrale des Heiligen Jakob in Šibenik wurde erstellt und mittels Zeitverlaufsanalysen untersucht. Die Ergebnisse weisen auf ein bedeutend nichtlineares Verhalten hin, das nicht einfach mit finiten Elementen erfasst werden kann. Ebenso deuten die Resultate auf kritische Stellen, so dass Bereiche maximaler Verschiebungen und Kontaktkräfte lokalisiert werden konnten.

Ključne riječi:

diskrete Elemente, nicht-glatte Kontaktdynamik, LMGC90, Kontaktgesetze, Gauss-Seidel

1. Introduction

Complex modelling and lack of adequate software are some of the reasons behind poor acceptance of discrete models in engineering practice. Although the finite element method (FEM) is a good mathematical model for describing the continuum, the discrete method is the preferred choice in the sphere of discontinuous media. The discrete method is based on defining geometry of individual elements, i.e. discrete elements and their mutual contact relationship.

In the territory of the Republic of Croatia, there are many buildings of exceptional cultural and historic significance that are built of stone blocks. Structures made of stone blocks without binder, or with poor binder, are considered to be discontinuous structural systems. St. James Cathedral in Šibenik is made of stone blocks without the use of binder, and it therefore belongs to the group of discontinuous systems. This paper focuses on the development of numerical model of the dome of St. James Cathedral in Šibenik, and on the response of this cathedral to seismic action. Numerical model was developed using the LMGC90 software, which is based on discrete formulation.

2. Discrete element method

The finite-element method (FEM) is widely accepted in all areas of engineering practice. The main property of the FEM is that it considers numerical model as a continuous medium. The geometry and behaviour of a continuous medium is described using pre-defined finite elements. Although behaviour of a great number of problems can be described using the FEM, the use must be made of the discrete element method (DEM) when a discontinuous or intermittent medium is considered. The discrete numerical model is described by a set of individual discontinuous media called discrete elements. They can be observed as absolutely rigid or deformable areas. If deformable discrete elements are considered, then the combined method called finite-discrete element method is used [1]. The finite-discrete element method is aimed at using advantages presented by the FEM and DEM. The interaction between individual discrete elements is described using contact laws.

Laws regulating contact between discrete elements can be defined by means of the smooth and non-smooth contact dynamics. The smooth dynamics attempts to describe deformable behaviour of discrete elements. Contacts between discrete elements are described by means of springs or functions. Behaviour at the contact can depend on the size of overlap, relative speed and relative force.

Spring-based modelling requires the use of time steps that should be smaller than the elastic time response so as to ensure numerical stability [2]. Rigid discrete elements require an increase in spring rigidity, and a shorter time step, which increases the time needed for analysis. Absolutely rigid materials require infinitesimal time steps. Smooth contact

dynamics is used for modelling materials with finite rigidity [2]. In the non-smooth contact dynamics, discrete elements are assumed to be absolutely rigid, while elastic behaviour between discrete elements is neglected [2].

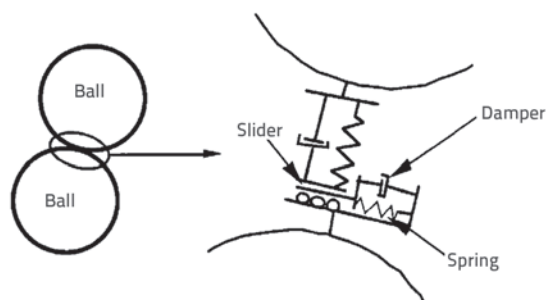


Figure 1. Model of the contact between discrete elements [2]

Unlike the smooth method, the non-smooth method enables the use of a greater time step and can describe "absolutely rigid materials". Proper attention must be paid to the selection of time step. A large time step may result in excessive penetration of discrete elements. An advantage of this method is that it converges quite well, which is otherwise a big problem in case of models with a large number of elements [2]. The non-smooth contact method is implemented in the program LMGC90, which is based on an open source code. The LMGC90 code is written in Fortran and C, and the programming language Python is used for entering the data. It should be noted that the program works exclusively with the operating system Linux, and supports the OpenMP, which enables computing in parallel.

2.1. Equation of motion of non-deformable discrete elements (DE)

Motion of non-deformable discrete elements is described in the Newton-Euler system of equations [3].

$$\begin{aligned} \mathbf{M}\dot{\mathbf{v}}^T &= \mathbf{p}(t) + \mathbf{r} \\ \mathbf{I}\dot{\boldsymbol{\omega}} &= \mathbf{m}(t) + \mathbf{m}_r \end{aligned} \tag{1}$$

Generalized coordinates \mathbf{q} define position of the centre of mass of discrete elements with respect to the origin of the Cartesian coordinate system. The speed of the centre of mass \mathbf{v}^T is defined by deriving coordinates \mathbf{q} along the time t .

$$\mathbf{v}^T = \dot{\mathbf{q}} \tag{2}$$

The speed of the discrete element's rotation around the centre of the mass is defined by means of $\boldsymbol{\omega}$. The values $\mathbf{p}(t)$ and $\mathbf{m}(t)$ describe external resulting force and external resulting moment. The matrices \mathbf{M} i \mathbf{I} define the mass matrix and the inertia matrix. The vectors \mathbf{r} and \mathbf{m}_r are the forces and moments that are caused by contact between two discrete elements.

2.2. Interaction of discrete elements

Each discrete element must have defined contours, interaction points, material characteristics and the law specifying behaviour at the place of contact. The contact of two discrete elements is realised between the selected interaction point and the closest point of the potential interaction body. The term *candidate*, which relates to the body whose interaction point is observed, is introduced to facilitate understanding. The term *antagonist*, representing the potential interaction body, is also introduced.

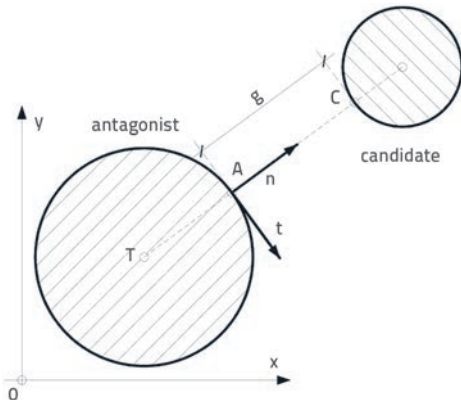


Figure 2. In-plane relation between candidate and antagonist

Figure 2 shows an in-plane problem of relationship between the *candidate* and *antagonist*. Points C and A are potential points of contact. Local axes are linked to the colliding body, while \mathbf{n} is normal to the tangential plane. To facilitate presentation, the problem is presented in two-dimensional space, but can simply be extended to three dimensions [3, 4].

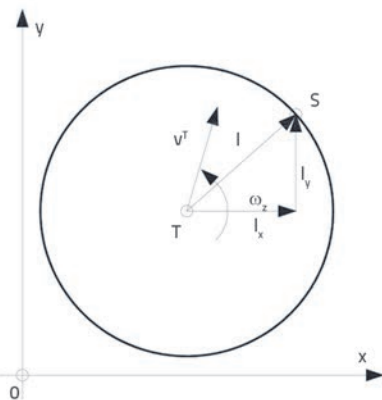


Figure 3. Motion of rigid discrete element

The motion of a rigid discrete element in x - y -plane is presented in Figure 3. Two points are defined. The point T represents the centre of the mass, while the point S is situated on the contour of the discrete element. The speed of the point S is defined by the speed of the centre of the mass \mathbf{v}_T and by angular velocity ω_z which is related to the rotation around the axis z . The velocity of the point S can be described by the following expression (3):

$$\begin{bmatrix} v^S_x \\ v^S_y \end{bmatrix} = \begin{bmatrix} 1 & 0 & -l_y \\ 0 & 1 & l_x \end{bmatrix} \begin{bmatrix} v^T_x \\ v^T_y \\ \omega_z \end{bmatrix} \tag{3}$$

The two-dimensional problem of the velocity of points on the contour of discrete elements can be extended to a three-dimensional problem, and the velocity of a point is then defined by the expression (4):

$$\mathbf{v}^S = \mathbf{v}^T + \boldsymbol{\omega} \times \mathbf{L} \tag{4}$$

where \mathbf{v}^S is the velocity vector in point S , \mathbf{v}^T is the velocity vector of the centre of mass, while $\boldsymbol{\omega}$ is the angular velocity vector. The matrix \mathbf{L} assumes the following form:

$$\mathbf{L} = \begin{bmatrix} 0 & l_z & -l_y \\ -l_z & 0 & l_x \\ l_y & -l_x & 0 \end{bmatrix} \tag{5}$$

It defines the relationship between the angular velocity $\boldsymbol{\omega}$ and velocity in point S . In Figure 3, the distance between the potential point of contact between two discrete elements is defined by the vector \mathbf{g} , and the change of vector \mathbf{g} in time defines relative velocity between discrete elements. From this point on, the relative velocity between discrete elements will be designated with \mathbf{U} . The velocities of potential points of contact between the *candidate* and the *antagonist* are defined in eq. (4), and their difference defines relative velocity as follows

$$\mathbf{U} = \mathbf{v}^T_C + \boldsymbol{\omega}_C \times \mathbf{L}_C - \mathbf{v}^T_A + \boldsymbol{\omega}_A \times \mathbf{L}_A \tag{6}$$

where \mathbf{v}^T_C and \mathbf{v}^T_A are the centre-of-mass velocities of the *candidate* and the *antagonist*, $\boldsymbol{\omega}_C$ and $\boldsymbol{\omega}_A$ are angular velocities of the *candidate* and the *antagonist*. Eq. (6) can be re-formulated as follows:

$$\mathbf{U} = [\mathbf{I} \quad \mathbf{L}_C - \mathbf{I} - \mathbf{L}_A] \begin{bmatrix} \mathbf{v}^T_C \\ \boldsymbol{\omega}_C \\ \mathbf{v}^T_A \\ \boldsymbol{\omega}_A \end{bmatrix} \tag{7}$$

or

$$\mathbf{U} = \mathbf{H}^T \mathbf{v} \tag{8}$$

where:

$$\mathbf{H}^T = [\mathbf{I} \quad \mathbf{L}_C - \mathbf{I} - \mathbf{L}_A] \tag{9}$$

The matrices \mathbf{L}_C and \mathbf{L}_A correspond to the matrix \mathbf{L} for potential points of contact between the *candidate* and the *antagonist* while \mathbf{I} is the unit matrix measuring 3×3 . Eq. (8) is the basic equation of the NSCD method, and it links relative velocities between the potential place of contact of two discrete elements and global

velocities of the same potential points of contact. The scalar product of Equation 8, with unit vector $[\bar{n}_\alpha \ \bar{i}_\alpha \ \bar{m}_\alpha]^T$ that defines the local coordinate system, transforms relative velocities in the direction of local axes, as shown in Figure 3. The index α denoting each potential contact in the system with several discrete elements is introduced. After transformation and introduction of the index α , the Expression 8 assumes the following form:

$$\mathbf{U}_\alpha = \mathbf{H}_\alpha^T \mathbf{v}_\alpha \tag{10}$$

The following relationship can also be established using Eq. (10):

$$\mathbf{r}_\alpha = \mathbf{H}_\alpha \mathbf{R}_\alpha \tag{11}$$

where \mathbf{r}_α is the contact force in the global system while \mathbf{R}_α is the contact force in the local system as defined according to contact law. \mathbf{H}_α^T is the transposed matrix \mathbf{H}_α [3].

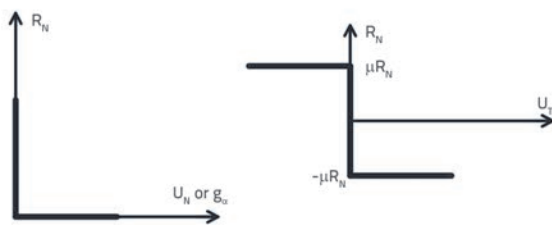


Figure 4. Signorini and Coulomb contact laws

Contact laws define relationships between the relative velocity or distance g and the contact force. Although there are many contact laws, the most frequently used ones are the Signorini and Coulomb laws, as shown in Figure 4. The Signorini's contact law is used to determine whether the contact between discrete elements has been realised. If the distance g is positive, the contact has not been realised, i.e. the normal contact force \mathbf{R}_N is equal to zero. When the distance g is equal to zero, then the normal contact force \mathbf{R}_N is activated, and it can assume infinite values [5]. The value of contact force \mathbf{R}_N depends on the value of forces acting on discrete elements [5]. For the model made of absolutely rigid discrete elements, the normal contact force \mathbf{R}_N is determined by means of impulses, and it depends on the relative velocity \mathbf{U}_N and on the selected value of time step Δt . The Signorini's law can be mathematically described using the following expressions:

$$\begin{aligned} g > 0 &\Rightarrow \mathbf{R}_N = 0 \\ g = 0 &\Rightarrow \mathbf{R}_N \geq 0 \end{aligned} \tag{12}$$

The Coulomb's contact law is shown in Figure 4. In case of dry friction, the value of friction force or tangential contact force \mathbf{R}_T depends on the friction coefficient μ and the normal contact force \mathbf{R}_N . The Coulomb's mathematical law can be presented as follows:

$$\begin{aligned} \mathbf{U}_T > 0 &\Rightarrow \mathbf{R}_T = -\mu \mathbf{R}_N \\ \mathbf{U}_T = 0 &\Rightarrow -\mu \mathbf{R}_N \leq \mathbf{R}_T \leq \mu \mathbf{R}_N \\ \mathbf{U}_T < 0 &\Rightarrow \mathbf{R}_T = \mu \mathbf{R}_N \end{aligned} \tag{13}$$

\mathbf{U}_T is the relative tangential velocity.

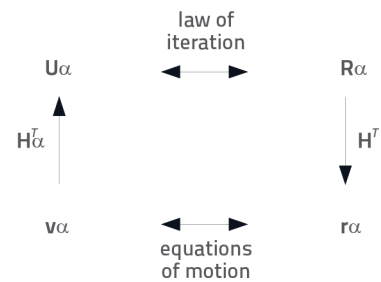


Figure 5. Relationship between global and local unknowns

The relationship between global and local unknowns is shown in Figure 5. Global unknowns are related to the centre of mass of a body or to network points. Global unknowns are displacements \mathbf{q} velocities \mathbf{v} , resulting forces and moments \mathbf{r} . Local unknowns are related to the distance between two bodies \mathbf{g} relative velocity between two bodies \mathbf{U} , and force \mathbf{R} .

3. Discrete model of the dome of St. James Cathedral in Šibenik

The drawings of the St. James Cathedral in Šibenik are kept at the Zagreb Institute of History and Art. Tracing-paper drawings on the scale of 1/200 and 1/50 are kept in the Institute's archives; digital versions are currently not available. These drawings consist of four façades, two longitudinal cross-sections, two transverse cross-sections, and the plan view of the structure. Longitudinal cross-sections are defined by planes crossing the cathedral along symmetry axis, and through the side nave. Cross-section planes cut the cathedral through three naves and the central part of the dome. The numerical model development does not require a "perfect" accuracy, i.e. several cm deviation from the as-built state will not significantly alter accuracy of the solution. Drawings on the scale of 1/200 are used in the scope of this paper. They are considered to be accurate enough for development of a good-quality numerical model. Visual inspection of the cathedral was also made, and it enabled collection of additional data for preparation of the model. This visual inspection enabled experts to determine regularity of placement of stone blocks, and the way in which steel ties are arranged.

3.1. Dome geometry

The dome is of octagonal form, and its sides measure 330 cm in length at the base. The height of the dome, measured from cornice to acroterion, amounts to 600 cm. The basic load-bearing system is formed of eight ribs that are linked together at the dome crown. The schematic view of the rib disposition is shown in Figure 6. The ribs are linked together with a central block connecting ribs into a single assembly. The central block and the ribs form an arch. The angle between two rib axes amounts to 45°. Each rib is made of ten elements. The rib height amounts to 55 cm along the entire rib length, while the rib width is variable. The rib width amounts to 50 cm at the spring level, and 38 cm at the crown [6].

After analysis of drawings, it was established that the rib shape can adequately be described by a parabola. It is defined by the rib axis equation.

$$z(x) = -\frac{h}{r^2}x^2 + h \quad [0,431] \quad (14)$$

The parabola is defined with two parameters h and r the value h defines the dome height, i.e. it represents the length between the origin and the crown of the parabola, while r is the radius of the octagon defining circle. The values of parameters h and r amount to 600,0 cm and 431,0 cm, respectively.

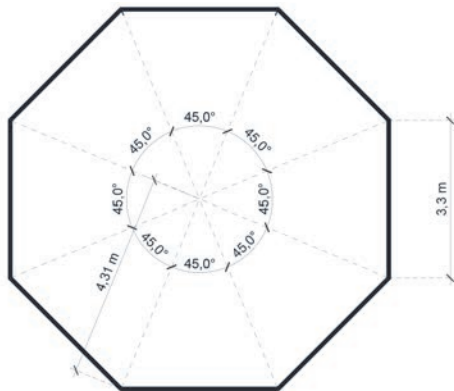


Figure 6. Disposition of rib axes

3.2. Ribs

After inspection of available documents, it was established that each rib is composed of ten segments of similar length, and so it was assumed that all segments are of equal length. The above assumption enables definition of conditions for the length and positioning of individual segments. The length and position of individual segments is defined by means of h , r , and r_1 , and by the number of segments. The parameter r_1 defines the size of the central stone, i.e. the rib start coordinate. To define the length of individual segments, it is first of all necessary to calculate the total length of parabola in the zone from r_1 to r . The total length of parabola in the zone from r_1 to r can be calculated using the following expression:

$$d_i(h, r, r_1) = 0,5r\sqrt{\frac{4h^2}{r^2} + 1} - 0,5r_1\sqrt{\frac{4h^2}{r^2} + 1} - \frac{0,25}{\sqrt{\frac{h^2}{r^2}}} \sinh^{-1}\left(2r_1\sqrt{\frac{h^2}{r^4}}\right) + \frac{0,25}{\sqrt{\frac{h^2}{r^2}}} \sinh^{-1}\left(\frac{2h^2}{r^3\sqrt{\frac{h^2}{r^4}}}\right) \quad (15)$$

Equation 6 is derived on the basis of the known arch length expression. The length of individual segments is defined by dividing the arch length with the number of segments. If the segment length is inserted instead of the total arch length in Expression 6, then the value of r , defining the end of the segment, can be calculated. The value of r was determined numerically using the program language Python, and the code calculating final coordinates of individual rib segments was written. The calculation result is the list of coordinates that will be designated below as x_i .

The rib cross section is defined with seventeen characteristic points. Coordinates of characteristic points are determined

from the reference point T_0 that is defined by the list of coordinates x_i , and by Expression 5. The remaining sixteen cross-section coordinates are defined using the pre-determined geometrical characteristics of the cross section and straight line perpendicular to the tangent of function 5 in point T_0 .

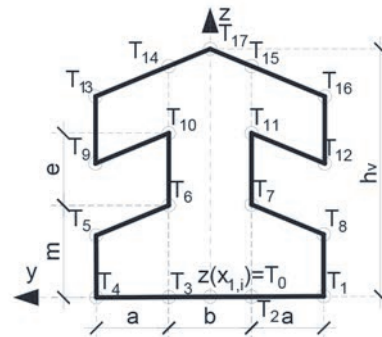


Figure 7. Approximation of cross-section

Cross-section parameters m , e , a , b and h_v change along the rib axis and must be calculated separately for each connection between two rib segments. To enable achievement of the desired cross-sectional shape, the rib segment is made of six four-sided prisms that behave as a single discrete element or as a rigid non-deformable body. The program defining the rib model was written. This program passes through two loops. One loop defines segments along the rib axis, and the other loop creates a new rib rotated for 45° .

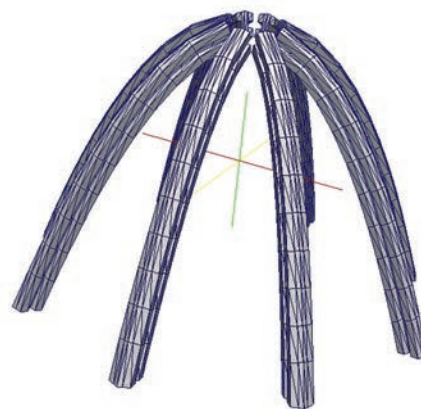


Figure 8. Rib model

3.3. Central stone (keystone)

The function of the keystone is to link ribs into a single whole, i.e. to obtain a properly closed structure. The keystone is modelled in such a way that it links several standard discrete elements into a single whole that behaves as a single absolutely rigid discrete element.

A keystone segment defined with eight points and twelve triangular zones is presented in Figure 9. A complete keystone model (presented in Figure 10) is created by rotation of the

segment shown in Figure 9. The rotation axis is situated in the origin of the coordinate system, i.e. it corresponds to the z axis.

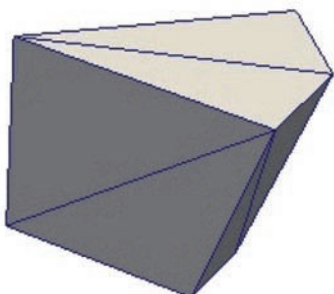


Figure 9. A keystone segment



Figure 10. A keystone model

3.4. Roofing

The dome roofing is made of trapezoidal stone blocks. The roofing blocks fill the space between the ribs and lean onto the ribs. Ribs have grooves into which roofing elements are inserted. At the contact of two roofing elements there is an overlap, the top plate passes over the bottom one. Roofing elements are curved in keeping with the curvature of the dome, Figure 11.

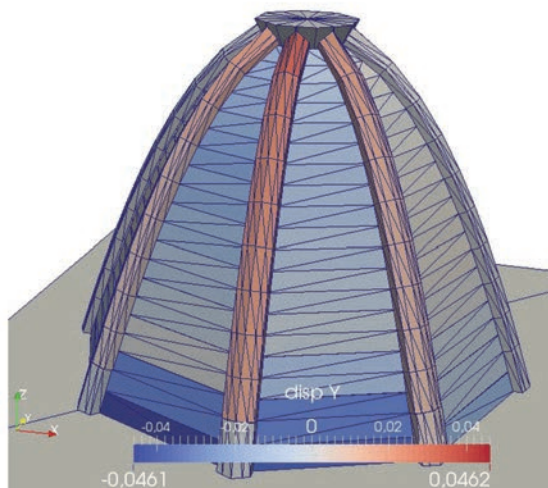


Figure 11. Discrete model of the dome of St. James Cathedral in Šibenik

It is very difficult to numerically define such a complex form of roofing elements. Therefore, model simplifications were introduced. Overlaps at the contact of two neighbouring roofing elements were neglected and the curvature was approximated with two areas. Individual roofing elements were defined through rib geometry. The geometry of one roofing element was defined in detail, and the remaining elements were obtained by means of a double loop. The first loop defines the elements along the ribs, and the second one the elements between neighbouring ribs.

4. Dynamic response of the dome

Two dynamic analyses are presented in the paper. The real data analysis was conducted according to the accelerogram for El Centro [7], which was increased using factors 1.5, 2.0, 2.5, and 3.0 so as to define full failure of the dome. The second analysis was conducted by means of five artificially generated earthquake records.

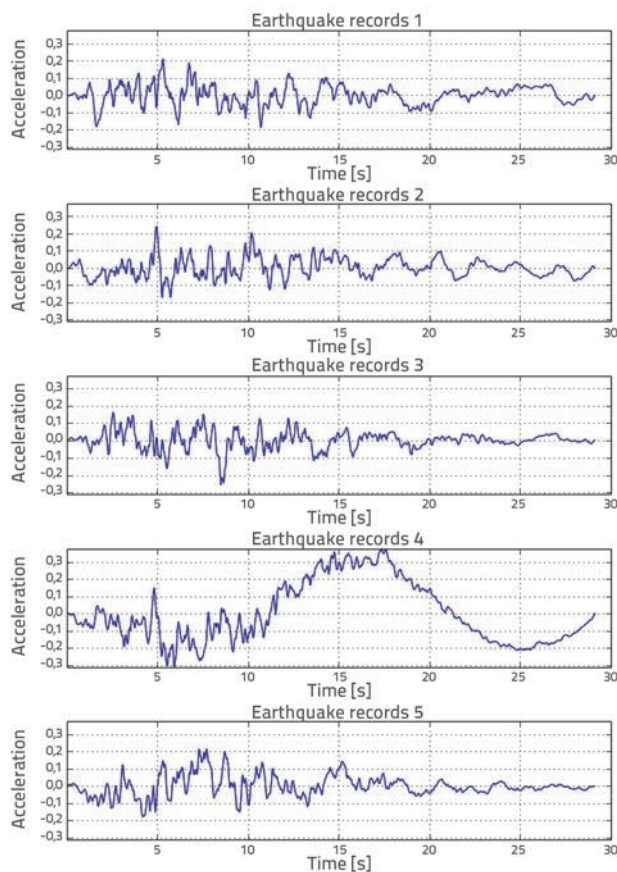


Figure 12. Artificially generated earthquake records

Earthquake records were generated using the Seismo Artif 2016 software [8, 9]. The elastic spectrum was defined according to EC8 [10] parameters that correspond to the location of St. James Cathedral in Šibenik.

The ground acceleration a_{gs} amounting to 0,19 g, was taken from the *Map of earthquake-prone areas in the Republic of Croatia* [11] for the soil category A and the return period of 475 years. The

building/structure significance factor of 1,4 was selected. The assumed distance from the epicentre is 10 km, and the average shear wave velocity is $v_{s,30} = 940$ m/s. The damping factor of 5% was assumed, and the assumed earthquake magnitude amounted to $M_s = 7,5$. Artificial seismic records were generated based on the elastic spectrum defined using the Seismo Artif 2016 software. The integration and correction, i.e. the baseline correction of the El Centro earthquake record and artificially generated records, was conducted using the Prisma software [12].

Two action types, force and velocity, were defined using the LMGC90 software. The integration and correction was made based on the known El Centro accelerations and artificially generated earthquake records, in order to obtain ground velocities or bases. The excitation was made in the x axis direction only, Figure 13.

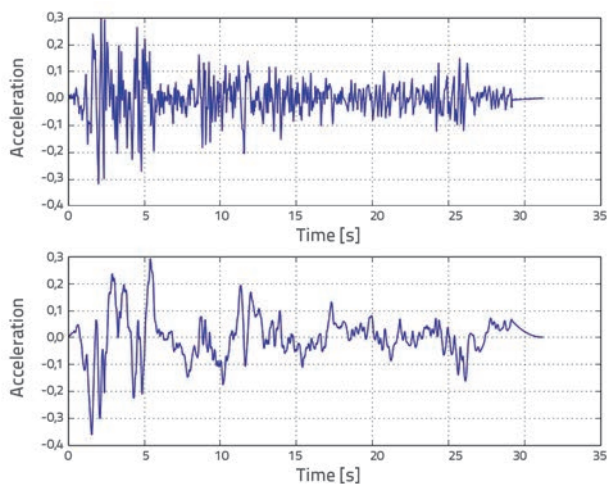


Figure 13. El Centro earthquake record

The iteration is made using the non-linear Gauss-Seidel method (NLGS). The system formed of two equations with two unknowns is assumed:

$$\begin{aligned} ax + by &= \lambda \\ cx + dy &= \delta \end{aligned} \quad (16)$$

It will be used to explain Gauss-Seidel methods. a , b , c , d , λ and δ are constant values. Eq. (16) can be re-formulated as follows:

$$\begin{aligned} x_{n+1} &= \frac{\lambda - by_n}{a} \\ y_{n+1} &= \frac{\delta - cx_n}{d} \end{aligned} \quad (17)$$

The iteration procedure is conducted by assuming initial values of x_0 and y_0 , which are inserted in Eq. (17). The new set of values is inserted in Eq. (16) and, if equations exhibit appropriate accuracy, the procedure is interrupted or values are re-inserted in Eq. (17). This iteration procedure is known as the Jacobi method. The Gauss-Seidel method is a modification of the Jacobi method: the same iteration pattern is used, except that

new values are used within the same iteration, i.e. as soon as a new value is known - it is used in calculation of the next value. It can be seen from Expression 18 that the value of x_{n+1} is used in the calculation of the value y_{n+1} .

$$\begin{aligned} x_{n+1} &= \frac{\lambda - by_n}{a} \\ y_{n+1} &= \frac{\delta - cx_{n+1}}{d} \end{aligned} \quad (18)$$

The same principle can also be applied to the system of nonlinear equations [13].

The number of iterations in LMGC90 software is defined with two parameters gs_it_1 and gs_it_2 [3]. The first loop, known as the control loop, is defined by the value of gs_it_2 . The control of accuracy is conducted in each step of the loop, i.e. it is determined whether the solution meets the accuracy criterion. If conditions of the required point are met, the iteration is interrupted. The second loop is the sub-loop of the first loop and is defined by the value of gs_it_1 . Unlike the first loop, the second loop can not interrupt the iteration once the desired accuracy is attained because the accuracy control is not made in every step of the iteration. The calculation time is thus reduced. The selected iteration parameters are presented in Table 1.

Table 1. Parameters selected for iteration procedure

Tolerance	Θ	Time step value	gs_it_1	gs_it_2
0,1666 ⁻³	0,5	0,002	2000	10

In his dissertation published in 2003, De Castro Oliveira determines the average coefficient of friction between stone blocks. The coefficient of friction to be used in this paper is set to $\mu = 0,62$ [14]. An average weight of stone is 2350 kN/m³ [15]. The results are presented using the ParaView software [16] which monitors structural changes over time. After analysis of results for the earthquake record El Centro, taking into account the magnification factor 1, it was established that permanent deformations occur due to shear between individual blocks. Remaining dome displacements are shown in Figure 11. It can easily be seen that nonlinear displacement occurs between the first and the second rows of rib elements. Figure 14 shows a relative relationship between the first two rows of the rib forming stone blocks for various earthquake record magnification factors according to the El Centro accelerogram. It can be seen from Figure 14 that the dome response after 6 seconds is such that relative displacements between the studied stone blocks assume a constant value for magnification factors of 2, 2.5, and 3. Further displacements are caused by dome opening i.e. by an increase of distance between individual ribs. This phenomenon can be seen in Figure 15, which shows a relative relationship between the bases of two ribs that are situated opposite to one another.

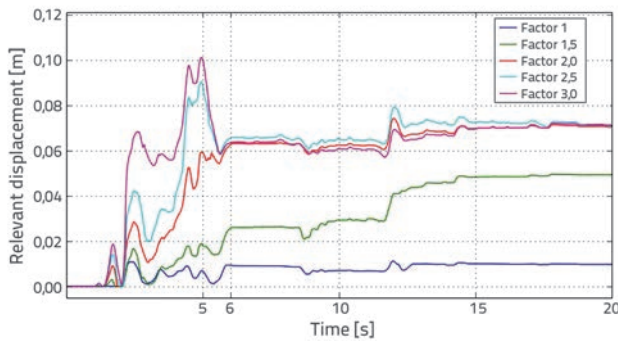


Figure 14. Relative displacements between the first two rows of rib-forming stone blocks for various earthquake-record magnification factors, according to El Centro accelerogram

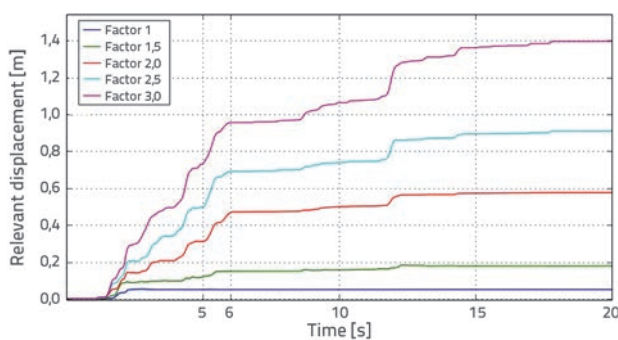


Figure 15. Correlation between two opposing ribs in their bases

The keystone push-out problem was also observed. In fact, a gradual push-out of the keystone occurs due to alternating change in direction of earthquake action. This may be due to the poorly defined geometry of the keystone and to poor definition of friction between blocks, although the possibility that this is the real dome behaviour can not be discarded. The keystone push-out phenomena are shown in Figure 16.

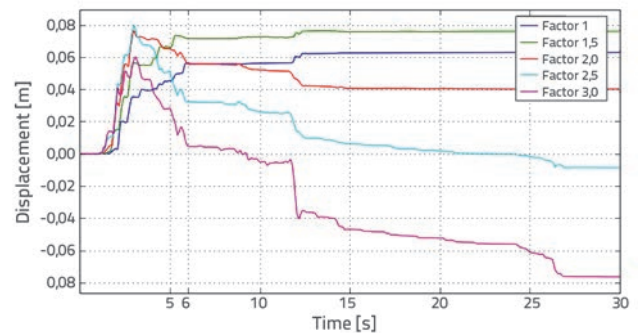


Figure 16. Dome keystone push-out for various earthquake record magnification factors, according to El Centro accelerogram

It can be seen from this figure that additional push-out after six seconds does not occur for factors 1 and 1.5. This interruption of keystone push-out is attributed to the reduction of acceleration i.e. to the ground acceleration in 6 seconds for the earthquake record according to the El Centro

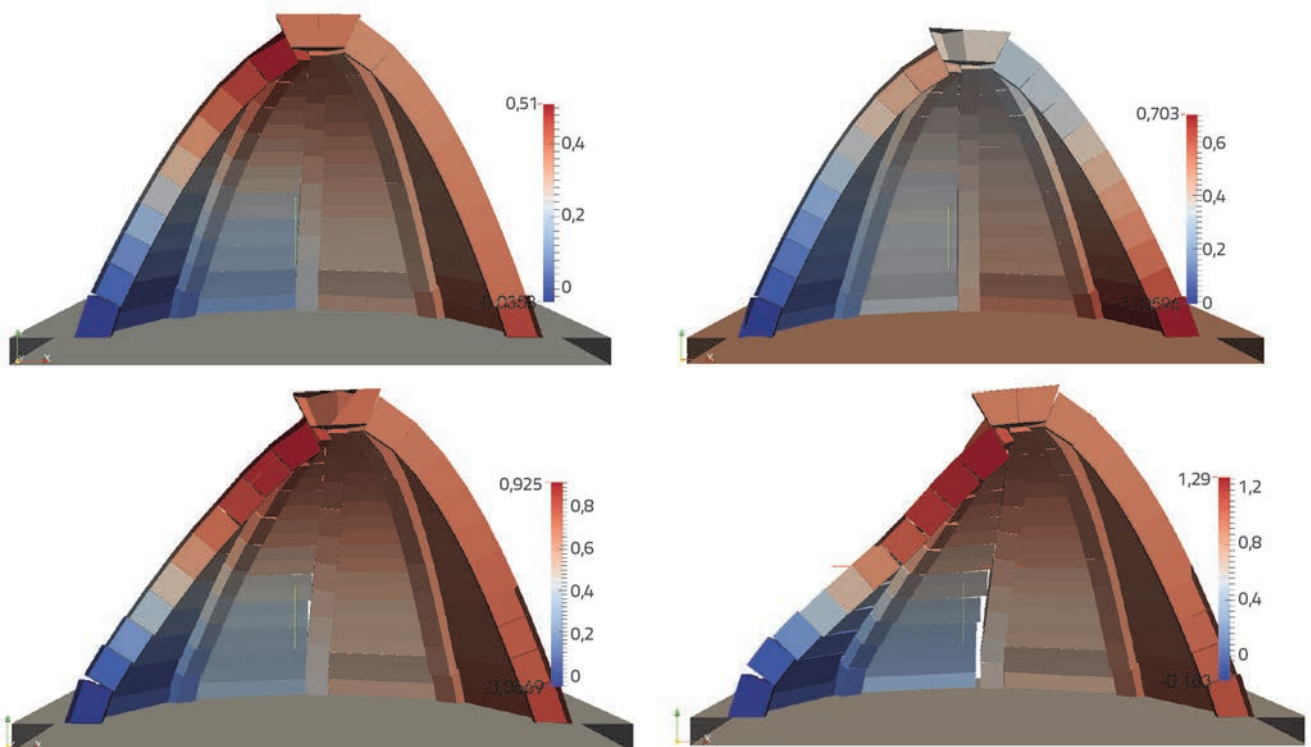


Figure 17. Dome response for El Centro earthquake action, magnified by three times

accelerogram, as shown in Figure 13. The dome keystone collapses (falls-through) after 6 seconds for factors 2, 2.5 and 3. This can be attributed to the rib separation phenomenon, as shown in Figure 16.

The interaction between individual blocks is shown in ParaViewer by means of dots, while the force value is designated by dot colour. It can be seen in Figure 18 that normal interaction forces are uniform along the ribs, and this situation remains unchanged throughout the earthquake action. Extreme values occur at the contact between the ribs and the support. Maximum value of the normal interaction force occurring in the dome model amounts to 43.2 kN. If it is assumed that the seating area is 50x50 mm, the stress at the contact amounts to 17,28 N/mm², which is less compared to the compressive strength of stone.

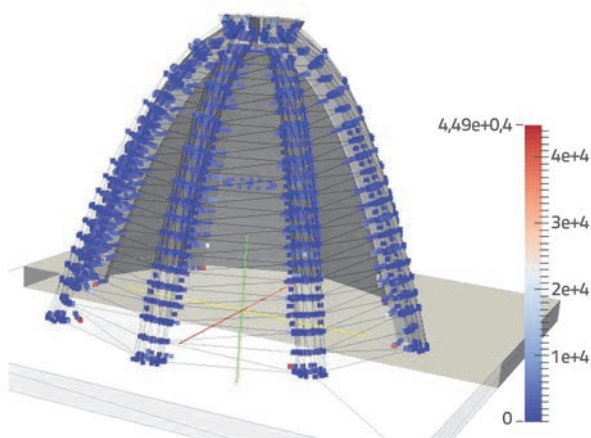


Figure 18. Normal interaction forces between stone blocks

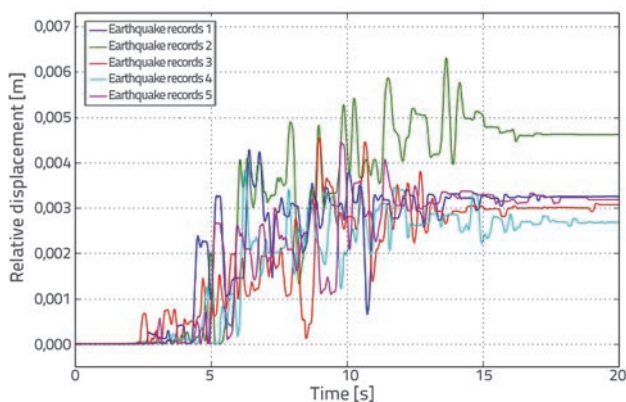


Figure 19. Relative displacements between the first two rows of rib-forming stone blocks for five artificially generated earthquake records

REFERENCES

- [1] Smoljanović, H.: Seizmička analiza zidanih konstrukcija metodom konačno-diskretnih elemenata, doktorski rad, Sveučilište u Splitu, 2013.
- [2] Hedman, S.: Smooth and non-smooth approaches to simulation of granular matter, magistarski rad, Umeå University, 2011.

The dome response was determined for artificially generated earthquake records. The El Centro earthquake record analysis pointed to critical points with regard to dome response, relative displacements between the first and the second rows of rib-forming stone blocks, and keystone push-out. The results presented in Figures 19 and 20 point to uniform behaviour of all five artificially generated earthquake records.

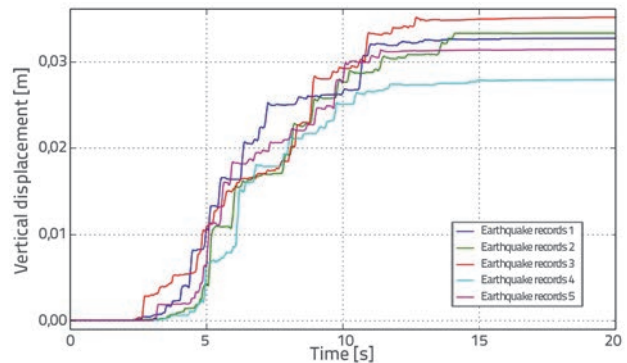


Figure 20. Dome keystone push-out for five artificially generated earthquake records

5. Conclusion

An approach to development of a discrete numerical model using the LMGC90 software based on the NSCD method is presented in the paper. The LMGC90 software does not have a graphical interface and so the model is described mathematically. The LMGC90 is based on an open source philosophy, which makes it a readily available program package.

Results obtained by dynamic analysis point to the problems of nonlinear behaviour of structures made of stone blocks. This nonlinearity is manifested in the shear or sliding between blocks, which is difficult to anticipate by means of the FEM. The model points to the keystone pushing-out problem, which may greatly affect stability of the structure, although additional investigations are needed in this respect.

Defining geometry by non-deformable discrete elements is a complex process. On the other hand, definition of material characteristics is quite simple. The stone weight and the coefficient of friction between individual blocks must be known. The research should be continued by expanding the model so as to comprise the entire cathedral, and by conducting experimental research with the purpose of obtaining good quality information about friction between individual discrete elements. In addition, development of model with deformable discrete elements might offer a better insight into the state of stress in individual blocks.

- [3] Dubios, F., Renouf, M.: Discrete Element Methods for the simulation of divided media, Laboratoire de Mécanique et Génie Civil, 2015.
- [4] Hibbeler, R. C.: Engineering Mechanics: Dynamics, Prentice Hall, 2012.
- [5] Acary, V., Jean, M.: Numerical simulation of monuments by the contact dynamics method, HAL (2009), pp. 69-78.
- [6] Čuzela, J.: Prilog obnovi kupole katedrale sv. Jakova u Šibeniku, Rad. Inst. povij. umjet. (1994), pp. 205–210.
- [7] Vibrationdata, <http://www.vibrationdata.com/elcentro.htm>, pristupljeno: 11.2.2015.
- [8] Seismo Artif 2016, <http://www.seismosoft.com/>, pristupljeno: 30.6.2016.
- [9] Seismo Artif 2016, http://www.seismosoft.com/Public/EditorUpload/Flash/SeismoArtifv2.1_GettingStarted.swf, pristupljeno: 30.6.2016.
- [10] Carvalho, E.: Eurocode 8 General rules and seismic actions, Dissemination of information workshop, Brussels, 2008.
- [11] Karte potresnih područja Republike Hrvatske, <http://seizkarta.gfz.hr/karta.php>, pristupljeno 31.6.2016.
- [12] Jeong, S., Lee, K., Jang, W.: PRISM for Earthquake Engineering A Program for seismic response analysis of SDOF system, Version 1.0.2, INHA University, 2011.
- [13] Gutiérrez, J.M., Magreñán, A.A., Varona, J.L.: The "Gauss-Seidelization" of iterative methods for solving nonlinear equations in the complex plane, Applied Math. Comp., 218 (2011), pp. 2467–2479, <http://dx.doi.org/10.1016/j.amc.2011.07.061>
- [14] De Casto Oliveira, D.V.: Experimental and numerical analysis of blocky masonry structures under cyclic loading, doktorski rad, Universidade do Minho, 2003.
- [15] Crnković, B., Šarić, Lj.: Građenje prirodnim kamenom, Sveučilište u Zagrebu, 1992.
- [16] ParaView, <http://www.paraview.org/paraview-guide/>, pristupljeno 30.6.2016.